Snapshot hyperspectral imaging with quantum correlated photons

Zhang, Yingwen; England, Duncan; Sussman, Benjamin

Publisher's version / Version de l'éditeur:
https://doi.org/10.1364/OE.462587
Optics Express, 31, 2, pp. 2282-2291, 2023-01-10

Research Article | Vol. 31, No. 2 / 16 Jan 2023 / Optics Express 2282
Optics EXPRESS

Snapshot hyperspectral imaging with quantum correlated photons

YINGWEN ZHANG,[1,2,*] DUNCAN ENGLAND,[1,4] AND BENJAMIN SUSSMAN[1,3]

[1]National Research Council of Canada, 100 Sussex Drive, K1A 0R6, Ottawa ON, Canada
[2]Nexus for Quantum Technologies, University of Ottawa, K1N 6N5, Ottawa ON, Canada
[3]Department of Physics, University of Ottawa, Ottawa, Ontario, K1N 6N5, ON, Ottawa ON, Canada
[4]duncan.england@nrc-cnrc.gc.ca
[*]yzhang6@uottawa.ca

Abstract: Hyperspectral imaging (HSI) has a wide range of applications from environmental monitoring to biotechnology. Conventional snapshot HSI techniques generally require a trade-off between spatial and spectral resolution and are thus limited in their ability to achieve high resolutions in both simultaneously. Most techniques are also resource inefficient with most of the photons lost through spectral filtering. Here, we demonstrate a proof-of-principle snapshot HSI technique utilizing the strong spectro-temporal correlations inherent in entangled photons using a modified quantum ghost spectroscopy system, where the target is directly imaged with one photon and the spectral information gained through ghost spectroscopy from the partner photon. As only a few rows of pixels near the edge of the camera are used for the spectrometer, effectively no spatial resolution is sacrificed for spectral. Also since no spectral filtering is required, all photons contribute to the HSI process making the technique much more resource efficient.

1. Introduction

Utilizing the properties of quantum entangled photons to enhance the performance of imaging techniques has been an active area of research in recent decades. Sub-shot noise imaging [1,2], quantum ghost imaging [3–5], imaging with undetected photons [6], and infra-red microscopy [7] are just some examples of the imaging techniques made possible by the unique properties of entangled photons. With recent improvements in source and detector technologies, these techniques are becoming increasingly practical, and integration timescales have improved from hours to minutes, or even seconds [8]. In this work, we showcase another advantage of quantum correlated imaging that may provide a viable alternative to classical methods. By applying the concepts of ghost spectroscopy [9–12] to quantum imaging, we show that snapshot hyperspectral imaging can be achieved by measuring the position of one photon from an entangled pair, and inferring its wavelength by making a spectral measurement on the other photon. With the use of a time-tagging camera, we demonstrate that a ~20 kilopixel image with ~2 nm spectral resolution over an 85 nm range can be achieved at the single photon level within a reasonable data acquisition time of between 1 to 5 minutes, depending on the type of target imaged.

Hyperspectral imaging (HSI) is a class of imaging techniques used to obtain the spectral information for each spatial location on an image and has a wide range of applications ranging from environmental and agricultural monitoring, biotechnology, medical diagnostics to food analysis [13–19]. Traditional HSI techniques rely on scanning either the spatial or spectral degree of freedom [20,21], and can provide high resolution in both position and spectrum, at the expense of long acquisition times due to the precision scanning required. Alternatively, so-called snapshot hyperspectral imaging (SHSI) techniques [22] can acquire spectral data in a single shot, by sacrificing spatial resolution. For example SHSI can be achieved using spectral filter arrays either directly on the camera sensor [23–25], or in conjunction with a microlens array [26–28]. In

#462587 https://doi.org/10.1364/OE.462587
Journal © 2023 Received 28 Apr 2022; revised 28 Nov 2022; accepted 16 Dec 2022; published 10 Jan 2023

Optics EXPRESS

these schemes, because an array of spectral pixels are required for each spatial pixel, a trade-off exists, and the spatial resolution is reduced in proportion to the desired spectral resolution. SHSI techniques without relying on spectral filter arrays have also been demonstrated, such as using the spatial and spectral correlations in speckle patterns [29], but the trade-off between the spatial and spectral information still exists. Compressive sensing techniques developed from coded aperture spectrometry has also been applied to snapshot hyperspectral imaging [30–33]. This technique does not require sacrificing spatial resolution for spectral, however the technique can be computational intensive and is prone to artifacts, though these issues has been greatly improved in recent years [33]. Finally, it is worth noting that, in terms of the number of photons collected, SHSI techniques and spectral scanning techniques can be resource inefficient. E.g. Photons arriving at the detector will be lost through spectral filtering and in the case of compressive sensing, at least half will be lost through the binary-coded mask. In the weak illumination regime, this inefficiency can lead to significantly increased integration time. Spatial scanning, though resource efficient, requires longer acquisition times to acquire a high resolution image due to mechanical scanning.

In our SHSI demonstration, we show that the issues with resolution and efficiency can be overcome by using entangled photon pairs. We will term this technique quantum correlation hyperspectral imaging (QCHSI). In QCHSI, we employ the temporal and spectral (anti)correlations in entangled photon pairs created through the process of spontaneous parametric down-conversion (SPDC). One photon, the *signal*, is sent to illuminate the target, which is imaged by a time-tagging camera. Its entangled partner photon, the *idler*, which had no interaction with the target, is sent onto a spectrometer built around the same camera. The photon pairs are then identified through a second order timing correlation measurement based on the photon detection times. Through this process, the spectral information at each pixel will automatically emerge as a result of the inherent spectral anti-correlation between the two photons. As the spectral information can be collected on just a few rows of pixels on the edge of the camera, effectively no spatial resolution is sacrificed in exchange for the spectral information. Furthermore, in this scheme, every photon within the HSI apparatus can contribute to the image, and none are removed by scanning or filtering. Hence the efficiency of the measurement is not fundamentally limited by the scheme and is only limited by practical considerations such as camera and grating efficiency.

2. Experimental setup

The experimental setup for QCHSI is shown in Fig. 1. A 405.5 nm continuous wave (CW) laser beam is focused onto a 1 mm thick Type 0 periodically poled potassium titanyl phosphate (ppKTP) crystal to generate, through the process of SPDC, temporally correlated and spectrally anti-correlated photon pairs, namely the signal and idler photons. The SPDC photons have a spectral bandwidth of ~100 nm centered around 811 nm. After filtering out the pump with a long-pass spectral filter, the SPDC beam is collimated by a 10 cm focal length lens. The signal and idler photons are then separated using a D-shaped mirror (a 50:50 beam-splitter can also be used here to create a circular shaped beam but at the cost of losing 50% of all coincidence events). The signal photons are used to illuminate a target sample which is then imaged onto the time-tagging camera (TPX3CAM [34,35]) where the arrival time and position of each photon is tagged. The idler photon is sent onto a spectrometer built around a diffraction grating, lens, and the camera.

The spectrometer is calibrated (see Supplement 1) so that pixel number can be mapped to wavelength, therefore we can tag both the arrival time and wavelength of each idler photon. The two photon beams are recombined, but slightly displaced, by a a half-wave plate rotated at 45 deg in one of the paths and a polarizing beam-splitter placed just before the camera, such that each beam will be imaged onto a different location of the camera. A 809 ± 41 nm spectral filter (Semrock FF01-809/81-25) is placed over the camera to block-off background light from

Optics EXPRESS

outside the spectral range of interest. The TPX3CAM is an event based time-tagging camera that has a spatial resolution of 256×256 pixels with a pixel pitch of $55\,\mu$m and an effective temporal resolution of ~ 7 ns on each pixel. We utilize this feature to time-tag every photon detected on each pixel and use this information to identify temporally correlated photon pairs between the different pixels, where one photon from the pair has interrogated the target, and the other has been diffracted by the grating. After identifying the coincident photons, the per-pixel spectral information of the sample will automatically emerge as a result of the inherent spectral anti-correlation between the signal and idler photons.

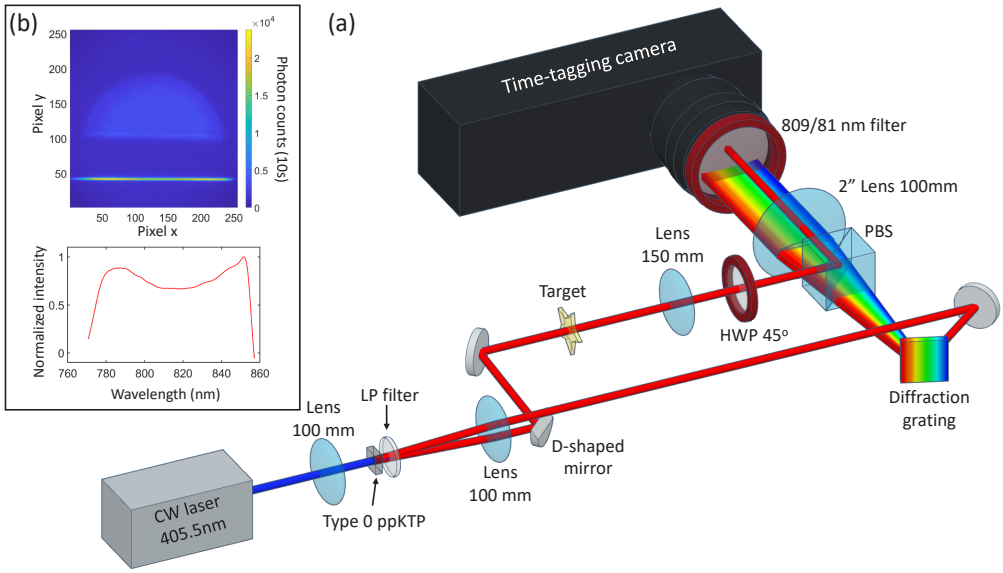

Fig. 1. (a) A 405.5 nm CW pump laser beam is focused onto a 1 mm thick Type 0 ppKTP crystal to generate temporal and spectrally (anti)correlated photon pairs. A long-pass (LP) spectral filter is used to filter out the pump laser. The generated photon pairs are first collimated by a lens before being split into two paths by a D-shaped mirror. The signal photon is sent to illuminate a target that is imaged onto the time-tagging camera. The idler photon is sent to a diffraction grating with the diffracted photons focused onto the camera by a lens, placed at one focal length from the grating and camera. The two photons are each imaged onto a different section of the camera with the aid of a polarizing beam-splitter (PBS) and a half-wave plate (HWP) rotated at 45° placed in the path of the signal photon. A 809 ± 41 nm spectral filter is placed over the camera to block-off background light from outside the spectral range of interest. (b) shows a raw image of the two beams captured on the camera accumulated over 10 seconds with no target present and the spectrum obtained from the cross-section of the spectrum arm. The semi-circular shape of the signal beam is due to the beam spit in half by the D-shaped mirror. Convolution of the SPDC spectrum with the instrument response (mainly from the grating, camera and the 809 ± 41 nm spectral filter) resulted in the shape of the idler spectrum.

After temporal coincidences are identified, the result is a 4-dimensional correlation data set $C^{\text{tot}}_{m,n}$ listing the total number of coincidence events measured between a pixel m of the signal beam and a pixel n of the idler beam (note that both m and n are two dimensional). To recover the spectral response of the target, some corrections need to be made. The first is to remove accidental coincidence events due to random detection overlap between uncorrelated photons. The expected number of accidental coincidences between pixels m and n is given by

$$C^{\text{acc}}_{m,n} = N_m N_n \tau, \tag{1}$$

Optics EXPRESS

where $N_{m(n)}$ is the total number of photons detected per second in pixel $m(n)$ and τ is the coincidence gating time, which for this experiment is set at 20 ns. The true number of coincidences can therefore be calculated simply by subtracting the expected accidental coincidence rate from the measured total:

$$C^{\text{true}}_{m,n} = C^{\text{tot}}_{m,n} - C^{\text{acc}}_{m,n}. \tag{2}$$

The second is that since the measured spectrum is of the idler photon and the two photon spectrum is anti-correlated, the coincidence spectrum obtained is in fact inverted from what is seen by the signal photon. This inversion is corrected using the energy conservation relation

$$\frac{1}{\lambda_p} = \frac{1}{\lambda_s} + \frac{1}{\lambda_i}, \tag{3}$$

where the λ_p, λ_s and λ_i are the wavelengths of the pump, signal and idler photons. The spectrum is then calibrated by matching the measured spectral shape to the fall-off edge of various spectral filters.

Finally, we note that, in common with all spectrometers, the spectrum determined after these corrections are convolutions of the target spectrum with the instrument response (mainly from the camera and grating), to correct for this will require a careful calibration of the detection system, which is beyond the scope the this work. More details on these corrections are outlined in the Supplement 1.

3. Results

As a proof of principle demonstration of QCHSI, we placed three different spectral band-pass filters - 786 ± 11 nm (Semrock FF01-786/22-25), 810 ± 5 nm (Semrock FF01-810/10-25) and 850 ± 5 nm (Semrock FF01-850/10-25) - in the path of the signal photon, their orientation with respect to the beam is shown in Fig. 2(a). Figure 2(b) shows a 2D projection of the background-subtracted 4D correlation data $C^{\text{true}}_{n,m}$ by summing over one of the indices, i.e. $C^{\text{true}}_{m} = \sum_n C^{\text{true}}_{m,n}$ for the signal beam image and $C^{\text{true}}_{n} = \sum_m C^{\text{true}}_{m,n}$ for the idler beam spectrum. C^{true}_{m} and C^{true}_{n} are then normalized separately and displayed on the same axes, i.e. $C^{\text{true}}_{m}/\max(C^{\text{true}}_{m}) + C^{\text{true}}_{n}/\max(C^{\text{true}}_{n})$, to better show the features in the signal image since the idler spectrum is much brighter. In this case no post-selection is applied and every coincident pair is included. Correspondingly, the spectrum shown in Fig. 2(c) is the average spectrum of the entire object.

In Fig. 2(d), we highlight regions of interest (ROIs) in the signal image corresponding to placing a filter in the 4D correlation data such that only coincidence events with the signal photon inside the ROI are considered. The resulting 2D projections clearly display the correlated idler spectrum, from which we can infer the transmission spectrum of the ROI using Eq. (3). The reverse is shown in Fig. 2(e), where a small ROI in the idler spectrum is selected. Here, only regions on the target with signal photons spectrally anti-correlated with the idler photons in the ROI will be lit up. For this target, an integration time of 100 s results in a signal-to-noise ratio (SNR) of ~ 5 for the brightest regions of the image.

In Fig. 3, a piece of paper with small punctured holes of ~0.2 mm in diameter is placed in front of the spectral filters to simulate a situation where the signal photons are reflected by or transmitted through very small targets (relative to the beam size). We see in Fig. 2(b) and (c) that due to the high noise from the small amount of transmitted signal photons, only a few bright spots can be seen on the target and features in the spectrum are also mostly washed out by noise. However, as seen in Fig. 2(d), if coincidences from just a few bright spots are considered, the spectrum can still be recovered with good visibility. On the other hand, as seen in Fig. 2(e), if only coincidences from a small ROI in the idler spectrum is considered, all points in the target with correlated wavelength is lit up, some of which are too faint to be visible in Fig. 2(b). For this target, an integration time of 275 s was required to achieve an SNR of >5 for the brightest spots.

Optics EXPRESS

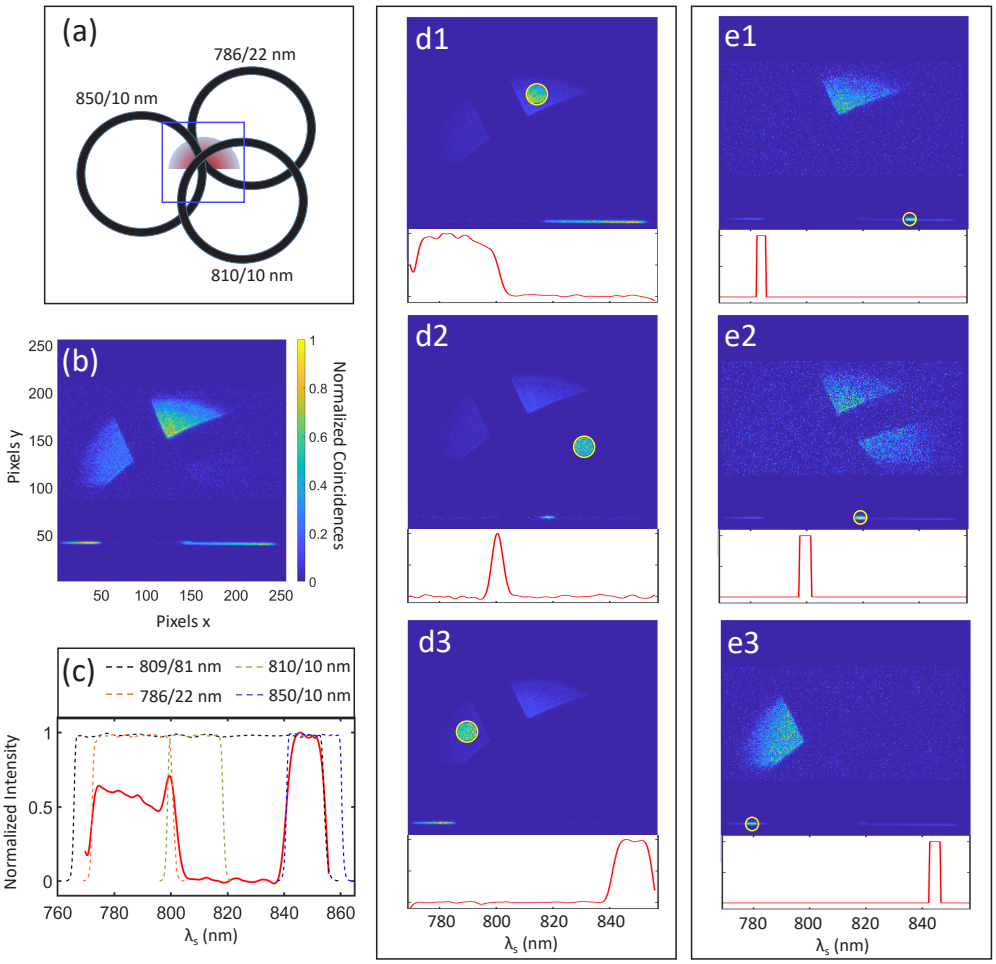

Fig. 2. a - Orientation of the 3 band-pass filters (786 ± 11 nm, 810 ± 5 nm, 850 ± 5 nm) with respect to the imaging beam. The blue square indicates the camera's field-of-view. b - Image of the twin beams after temporal correlation analysis. c - Average signal photon spectrum as calculated by energy conservation with the dashed lines showing the transmission region of the various filters placed in the beam path. d1-d3 - Correlated spectrum of selected regions (highlighted by the yellow circle) in the imaging signal arm with the corresponding signal photon spectrum shown in the insets. As reference, a faint background of the full beam is shown in the images. e1-e3 Correlated image of selected regions (highlighted by the yellow circle) in the spectrometer arm with the insets showing the corresponding wavelength window selected for the signal photon. A faint background of the full correlated spectrum is shown in the images as reference. Data acquisition time is 100 s and all displayed images and spectrum are background subtracted. As the maximum intensity of the idler spectrum is much brighter than the signal beam, the two are normalized separately in all the displayed images in order to make features in the signal beam more visible. The displayed signal spectrum have been smoothed through a cubic spline.

Optics EXPRESS

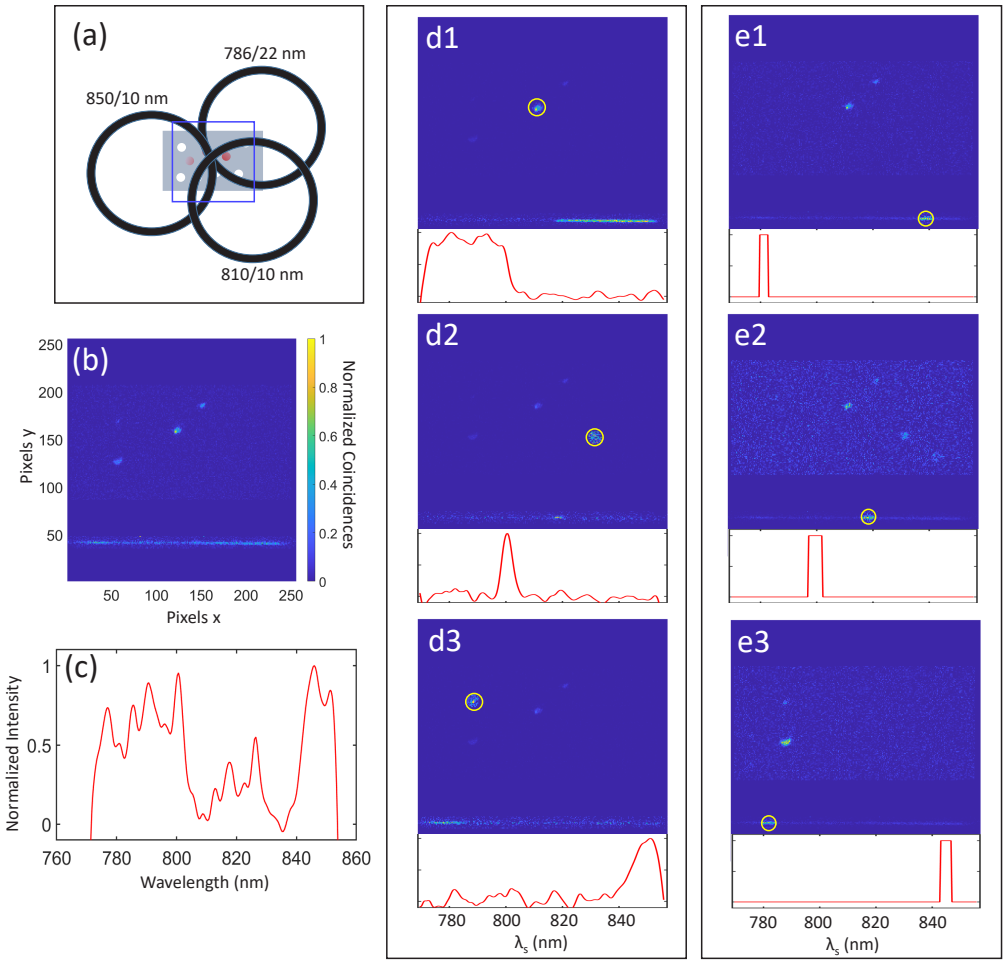

Fig. 3. a - Orientation of the 3 band-pass filters (786 ± 11 nm, 810 ± 5 nm, 850 ± 5 nm) with respect to the imaging beam. Over the beam is a piece of paper with small punctured holes of ~0.2 mm in diameter. The blue square indicates the camera's field-of-view. b - Image of the twin beams after time correlation analysis. c - Average signal photon spectrum as calculated by energy conservation. d1-d3 - Correlated spectrum of selected regions (highlighted by the yellow circle) in the imaging signal arm with the signal spectrum shown in the insets. As reference, a faint background of the full beam is shown in the images. e1-e3 Correlated image of selected regions (highlighted by the yellow circle) in the spectrometer arm with the insets showing the corresponding wavelength window selected for the signal photon. A faint background of the full correlated spectrum is shown in the images as reference. Data acquisition time is 275 s and all displayed images and spectrum are background subtracted. As the maximum intensity of the idler spectrum is much brighter than the signal beam, the two are normalized separately in all the displayed images in order to make features in the signal beam more visible. The displayed signal spectrum have been smoothed through a cubic spline.

Optics EXPRESS

4. Discussion

The spectral resolution of the QCHSI technique is determined by the bandwidth of the pump laser and the resolution of the spectrometer. In this case, the pump is a narrow linewidth continuous wave laser so the resolution limit is dominated by the spectrometer setup. Based on the thickness of the spectral band (3 pixels wide) and the width of the spectral peak in the overlap region between the 786 ± 11 nm and 810 ± 5 nm filters (~2 nm FWHM), we estimate the spectral resolution of our system to be ~2 nm maximum. In a previous experiment [36], where the same SPDC source was used, a resolution of 0.7 nm was achieved with the SPDC photons first coupled into single mode fibers before sent onto the spectrometer. This was also approximately the theoretical limit of this SPDC source as calculated in [36]. Some improvements to the current setup can be made in order to try reach the theoretical limit, such as tighter focusing of the pump beam onto the crystal or expanding the idler beam size at the grating. Coupling the idler beam into a single mode fiber can also be done, however this will come with significant losses from fiber coupling and reduce the field of view in the signal beam. To overcome the theoretical spectral resolution limit of 0.7 nm, the SPDC source can be improved by either using a longer crystal or using a narrower linewidth laser.

The demonstrated QCHSI system has a spectral resolution of ~ 2 nm over a 80 nm range, resolving 40 distinct spectral bins. The quantum efficiency of the camera is ~7% [37], and coincident detection of 2 photons means that the total efficiency is only ~ 0.5%. For comparison, a conventional system with 40 spectral filters and a high efficiency (>90%) CMOS camera would have an efficiency of $\gtrsim$ 2%. So, in the present demonstration, QCHSI is an order of magnitude less efficient than an analagous classical approach and requires minute-scale integration times. However, due to the quadratic efficiency scaling for coincidence detection, only modest improvements in measurement efficiency are required to make QCHSI more effective: for example, if a camera efficiency of 15% were achievable, the 2 photon coincidence efficiency would be ~ 2%, matching the classical ideal analogue. Moreover, with high efficiency (>50%), high spatial-temporal resolution (>1 Megapixel, ~ 100 ps timing resolution) SPAD array camera technology expected to be commercially available soon [38,39], we expect real-time spectral imaging with QCHSI will be possible, with an order of magnitude higher photon efficiency than classical approaches.

In this initial demonstration, type-0 degenerate SPDC was used such that each photon mode is centred at 810 nm, with a spectral bandwidth of ~100 nm. The bandwidth could be further increased by reducing the crystal thickness for larger spectral coverage or, for increased spectral resolution, narrower bandwidth photons could be generated by type-II SPDC. Furthermore, non-degenerate pair sources could be used to interrogate samples in very different spectral windows [40]. In this demonstration, the same camera is used for both the image and the spectrum for simplicity. But, more generally, the spectral information could be obtained using a second camera, or a separate device such as a 1D avalanche photo-diode array [41], or a time-of-flight fiber spectrometer [42]. Finally, we note that QCHSI could also be operated in ghost imaging mode, where the target is placed in the spectrometer arm instead of the imaging arm, however it can be difficult to accurately find the image plane of the “ghost" target in the imaging arm using this approach.

Though there are significant potential advantages of using QCHSI, there are still inherent limitations in the technique which cannot be solved by improved detectors. Principally, QCHSI is an active imaging technique where the target must be illuminated with quantum correlated photons generated by the observer, it cannot work passively using background light. Most conventional SHSI techniques can work both with active and passive illumination. Secondly, QCHSI it is not suitable for imaging fluorescent targets because the wavelength change imparted by fluoresence in the signal arm will not be detected by observing the idler arm.

Optics EXPRESS

Our demonstration can potentially be performed using classical ghost spectroscopy which has been demonstrated in recent years, using either the spectral correlation present in specialized thermal sources [11] or through computational methods using a programmable spectral filter [12]. Due to the nature of classical ghost spectroscopy needing to scan hundreds of spectral patterns, we expect the data acquisition time will be similar to that presented in this work.

5. Conclusion

In conclusion, we have demonstrated a proof of concept SHSI system utilizing the strong temporal and spectral (anti)correlations inherent in entangled photon pairs generated through the process of SPDC. With this system, almost no spatial resolution will need to be sacrificed in exchange for the spectral as in most conventional SHSI techniques, permitting for the maximum spatial and spectral resolution allowed by the detection camera and imaging system to be achieved simultaneously. In addition, the strong temporal correlation inherent in the SPDC photons also offer high noise tolerance, a feature well studied in quantum lidars and other imaging works [43–46]. Utilizing the noise resistant feature provided by the temporal correlation measurement and the higher photon efficiency of the technique (no photon losses through scanning or spectral filtering) makes this technique well suited for applications requiring weak illumination such as covert illumination or imaging of light sensitive samples. Due to limitations in detection technology, the performance of QCHSI is currently still far from matching commercial SHSI cameras in terms of spatial resolution and data acquisition time, but we believe this issue can be overcome in the near future with the advent of improved single photon detection technologies [38,39,47,48].

Funding. Defence Research and Development Canada.

Acknowledgements. The authors are grateful to Antony Orth, Andrew Ridsdale, Denis Guay, and Doug Moffatt for stimulating discussions and technical support. This work was partly supported by Defence Research and Development Canada.

Disclosures. The authors declare no conflicts of interest.

Data availability. The raw data underlying the results presented in this paper are not publicly available at this time due to its size but may be obtained from the authors upon reasonable request.

Supplemental document. See Supplement 1 for supporting content.

References

1. G. Brida, M. Genovese, and I. Ruo Berchera, "Experimental realization of sub-shot-noise quantum imaging," Nat. Photonics **4**(4), 227–230 (2010).
2. N. Samantaray, I. Ruo-Berchera, A. Meda, and M. Genovese, "Realization of the first sub-shot-noise wide field micscope," Light: Sci. Appl. **6**(7), e17005 (2017).
3. T. B. Pittman, Y. H. Shih, D. V. Strekalov, and A. V. Sergienko, "Optical imaging by means of two-photon quantum entanglement," Phys. Rev. A **52**(5), R3429–R3432 (1995).
4. J. H. Shapiro and R. W. Boyd, "The physics of ghost imaging," Quantum Inf. Process. **11**(4), 949–993 (2012).
5. M. J. Padgett and R. W. Boyd, "An introduction to ghost imaging: quantum and classical," Philos. Transactions Royal Soc. Lond. A: Math. Phys. Eng. Sci. **375**, 20160233 (2017).
6. G. B. Lemos, V. Borish, G. D. Cole, S. Ramelow, R. Lapkiewicz, and A. Zeilinger, "Quantum imaging with undetected photons," Nature **512**(7515), 409–412 (2014).
7. A. V. Paterova, S. M. Maniam, H. Yang, G. Grenci, and L. A. Krivitsky, "Hyperspectral infrared microscopy with visible light," Sci. Adv. **6**(44), eabd0460 (2020).
8. Y. Zhang, A. Orth, D. England, and B. Sussman, "Ray tracing with quantum correlated photons to image a three-dimensional scene," Phys. Rev. A **105**(1), L011701 (2022).
9. G. Scarcelli, A. Valencia, S. Gompers, and Y. Shih, "Remote spectral measurement using entangled photons," Appl. Phys. Lett. **83**(26), 5560–5562 (2003).
10. A. Yabushita and T. Kobayashi, "Spectroscopy by frequency-entangled photon pairs," Phys. Rev. A **69**(1), 013806 (2004).
11. P. Janassek, S. Blumenstein, and W. Elsäßer, "Ghost spectroscopy with classical thermal light emitted by a superluminescent diode," Phys. Rev. Appl. **9**(2), 021001 (2018).
12. P. Ryczkowski, C. G. Amiot, J. M. Dudley, and G. Genty, "Experimental demonstration of spectral domain computational ghost imaging," Sci. Rep. **11**(1), 8403 (2021).

Optics EXPRESS

13. G. Lu and B. Fei, "Medical hyperspectral imaging: a review," J. Biomed. Opt. **19**(09), 1–24 (2014).
14. C. P. Bacon, Y. Mattley, and R. DeFrece, "Miniature spectroscopic instrumentation: Applications to biology and chemistry," Rev. Sci. Instrum. **75**(1), 1–16 (2004).
15. A. Gowen, C. O'Donnell, P. Cullen, G. Downey, and J. Frias, "Hyperspectral imaging–an emerging process analytical tool for food quality and safety control," Trends Food Sci. Technol. **18**(12), 590–598 (2007).
16. A. Orth, M. J. Tomaszewski, R. N. Ghosh, and E. Schonbrun, "Gigapixel multispectral microscopy," Optica **2**(7), 654–662 (2015).
17. T. Slonecker, G. B. Fisher, D. P. Aiello, and B. Haack, "Visible and infrared remote imaging of hazardous waste: A review," Remote Sens. **2**(11), 2474–2508 (2010).
18. S. Delalieux, A. Auwerkerken, W. W. Verstraeten, B. Somers, R. Valcke, S. Lhermitte, J. Keulemans, and P. Coppin, "Hyperspectral reflectance and fluorescence imaging to detect scab induced stress in apple leaves," Remote Sens. **1**(4), 858–874 (2009).
19. K. Zhu, Z. Sun, F. Zhao, T. Yang, Z. Tian, J. Lai, B. Long, and S. Li, "Remotely sensed canopy resistance model for analyzing the stomatal behavior of environmentally-stressed winter wheat," ISPRS J. Photogramm. Remote. Sens. **168**, 197–207 (2020).
20. R. O. Green, M. L. Eastwood, C. M. Sarture, T. G. Chrien, M. Aronsson, B. J. Chippendale, J. A. Faust, B. E. Pavri, C. J. Chovit, M. Solis, M. R. Olah, and O. Williams, "Imaging spectroscopy and the airborne visible/infrared imaging spectrometer (aviris)," Remote. Sens. Environ. **65**(3), 227–248 (1998).
21. N. Gat, "Imaging spectroscopy using tunable filters: a review," in *Wavelet Applications VII*, vol. 4056 H. H. Szu, M. Vetterli, W. J. Campbell, and J. R. Buss, eds., International Society for Optics and Photonics (SPIE, 2000), pp. 50–64.
22. N. A. Hagen and M. W. Kudenov, "Review of snapshot spectral imaging technologies," Opt. Eng. **52**(9), 090901 (2013).
23. P.-J. Lapray, X. Wang, J.-B. Thomas, and P. Gouton, "Multispectral filter arrays: Recent advances and practical implementation," Sensors **14**(11), 21626–21659 (2014).
24. Z. Wang, S. Yi, A. Chen, M. Zhou, T. S. Luk, A. James, J. Nogan, W. Ross, G. Joe, A. Shahsafi, K. X. Wang, M. A. Kats, and Z. Yu, "Single-shot on-chip spectral sensors based on photonic crystal slabs," Nat. Commun. **10**(1), 1020 (2019).
25. K. Monakhova, K. Yanny, N. Aggarwal, and L. Waller, "Spectral diffusercam: lensless snapshot hyperspectral imaging with a spectral filter array," Optica **7**(10), 1298–1307 (2020).
26. R. Shogenji, Y. Kitamura, K. Yamada, S. Miyatake, and J. Tanida, "Multispectral imaging using compact compound optics," Opt. Express **12**(8), 1643–1655 (2004).
27. S. A. Mathews, "Design and fabrication of a low-cost, multispectral imaging system," Appl. Opt. **47**(28), F71–F76 (2008).
28. R. Horstmeyer, G. Euliss, R. Athale, and M. Levoy, "Flexible multimodal camera using a light field architecture," in *2009 IEEE International Conference on Computational Photography (ICCP)*, (2009), pp. 1–8.
29. S. K. Sahoo, D. Tang, and C. Dang, "Single-shot multispectral imaging with a monochromatic camera," Optica **4**(10), 1209–1213 (2017).
30. S. B. Mende, E. S. Claflin, R. L. Rairden, and G. R. Swenson, "Hadamard spectroscopy with a two-dimensional detecting array," Appl. Opt. **32**(34), 7095–7105 (1993).
31. A. A. Wagadarikar, N. P. Pitsianis, X. Sun, and D. J. Brady, "Video rate spectral imaging using a coded aperture snapshot spectral imager," Opt. Express **17**(8), 6368–6388 (2009).
32. Q. Zhang, R. Plemmons, D. Kittle, D. Brady, and S. Prasad, "Joint segmentation and reconstruction of hyperspectral data with compressed measurements," Appl. Opt. **50**(22), 4417–4435 (2011).
33. I. Choi, D. S. Jeon, G. Nam, D. Gutierrez, and M. H. Kim, "High-quality hyperspectral reconstruction using a spectral prior," ACM Trans. Graph. **36**(6), 1–13 (2017).
34. A. Nomerotski, "Imaging and time stamping of photons with nanosecond resolution in timepix based optical cameras," Nucl. Instrum. Methods Phys. Res., Sect. A **937**, 26–30 (2019).
35. https://www.amscins.com/tpx3cam/,.
36. Y. Zhang, D. England, A. Nomerotski, and B. Sussman, "High speed imaging of spectral-temporal correlations in hong-ou-mandel interference," Opt. Express **29**(18), 28217–28227 (2021).
37. V. Vidyapin, Y. Zhang, D. England, and B. Sussman, "Characterisation of a single photon event camera for quantum imaging," (2022).
38. K. Morimoto, A. Ardelean, M.-L. Wu, A. C. Ulku, I. M. Antolovic, C. Bruschini, and E. Charbon, "Megapixel time-gated spad image sensor for 2d and 3d imaging applications," Optica **7**(4), 346–354 (2020).
39. https://global.canon/en/news/2021/20211215.html,.
40. R. S. Aspden, N. R. Gemmell, P. A. Morris, D. S. Tasca, L. Mertens, M. G. Tanner, R. A. Kirkwood, A. Ruggeri, A. Tosi, R. W. Boyd, G. S. Buller, R. H. Hadfield, and M. J. Padgett, "Photon-sparse microscopy: visible light imaging using infrared illumination," Optica **2**(12), 1049–1052 (2015).
41. K. D. Johnsen, P. Kolenderski, C. Scarcella, M. Thibault, A. Tosi, and T. Jennewein, "Time and spectrum-resolving multiphoton correlator for 300–900nm," J. Appl. Phys. **116**(14), 143101 (2014).
42. M. Avenhaus, A. Eckstein, P. J. Mosley, and C. Silberhorn, "Fiber-assisted single-photon spectrograph," Opt. Lett. **34**(18), 2873–2875 (2009).

Optics EXPRESS

43. D. G. England, B. Balaji, and B. J. Sussman, "Quantum-enhanced standoff detection using correlated photon pairs," Phys. Rev. A **99**(2), 023828 (2019).
44. H. Liu, D. Giovannini, H. He, D. England, B. J. Sussman, B. Balaji, and A. S. Helmy, "Enhancing lidar performance metrics using continuous-wave photon-pair sources," Optica **6**(10), 1349–1355 (2019).
45. T. Gregory, P.-A. Moreau, E. Toninelli, and M. J. Padgett, "Imaging through noise with quantum illumination," Sci. Adv. **6**(6), eaay2652 (2020).
46. J. Zhao, A. Lyons, A. C. Ulku, H. Defienne, D. Faccio, and E. Charbon, "Light detection and ranging with entangled photons," Opt. Express **30**(3), 3675–3683 (2022).
47. https://instrumentationseminar.desy.de/sites2009/site_instrumentationseminar/content/e70397/e310935/,.
48. A. Nomerotski, P. Stankus, and A. Slosar, *et al.*, "Quantum-assisted optical interferometers: instrument requirements," in *Optical and Infrared Interferometry and Imaging VII*, vol. 11446 P. G. Tuthill, A. Mérand, and S. Sallum, eds., International Society for Optics and Photonics (SPIE, 2020), pp. 290–306.